Artificial Spectrin Shells Reconstituted on Giant Vesicles

ARTICLE *in* JOURNAL OF PHYSICAL CHEMISTRY LETTERS · MAY 2012

Impact Factor: 7.46 · DOI: 10.1021/jz300377q

3 AUTHORS:

Ivan Lopez-Montero
Complutense University of Madrid
36 PUBLICATIONS **606** CITATIONS
SEE PROFILE

Ruddi Rodríguez-García
Utrecht University
8 PUBLICATIONS **95** CITATIONS
SEE PROFILE

Francisco Monroy
Complutense University of Madrid
103 PUBLICATIONS **1,590** CITATIONS
SEE PROFILE

THE JOURNAL OF PHYSICAL CHEMISTRY Letters

Letter

pubs.acs.org/JPCL

Artificial Spectrin Shells Reconstituted on Giant Vesicles

Iván López-Montero,* Ruddi Rodríguez-García, and Francisco Monroy*

Mechanics of Biological Systems and Department of Physical Chemistry I, Universidad Complutense, 28040 Madrid, Spain

Supporting Information

ABSTRACT: In the experimental approach to a synthetic minimal cell, the membrane compartment is a main component. Lipid vesicles represent the natural host for the artificial reconstruction of a cytomimetic membrane skeleton able to support mechanical function. Using the membrane component of human erythroid cells, we have reconstructed a membrane shell composed of a spectrin skeleton and fed by ATP. The structural and mechanical analysis reveals this spectrin skeleton as topological network supporting mechanical rigidity. Such an artificial shell would define a membrane compartment mechanically stable under physiological conditions.

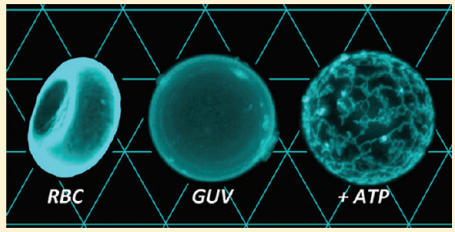

SECTION: Biomaterials, Surfactants, and Membranes

Cytoskeleton shells are complex biosystems known to self-assemble spontaneously from simple components.[1] Each building block of these membrane structures has evolved specific interactions with the component it connects to so entailing an enhanced function connected to their evolutively optimized structure. Expanding on these principles, the construction of a cytomimetic membrane skeleton supporting mechanical function is now conceivable.[2] This can be achieved by synthetic integration of building blocks, small molecules, and exogenous conditions existing in a native cell.[2−6] Previously, different molecular reconstitutions of membrane cortexes have been achieved in giant unilamellar vesicles.[7−13] However, no defined skeleton structures were obtained, the controlled construction of a topological shell with reinforced- mechanical function remaining still a challenge. In this Letter, we report the first artificial reconstruction of a topological shell based on the erythroid membrane cytoskeleton. Differently to bottom-up minimal reconstitutions using single components, our approach is top-down, dealing with the reconstruction of an artificial vesicle object from a membrane extract containing all of the relevant molecular components. These artificial shells are biochemically and structurally similar to the cytoskeleton network observed in vitro[14,15] and represent the first synthetic assembly of a rigid membrane with a skeleton structure. In vertebrates, spectrin is the major component of the erythrocyte cytoskeleton, a rigid mesh structure providing the red blood cell (RBC) with the mechanical resistance necessary to survive under bloodstream flow.[1] On a molecular level, long-range interactions enable the assembly of spectrin with specific components (actin and ankyrin, principally) through supramolecular connections occurring at specific nodes in the network.[14,15] This construction underlies a "goldilocks" principle by which the assembly interactions must fall within certain margins, as opposed to reaching extremes, where construction simply fails.[16−18] Consequently, a cytomimetic shell could be eventually reconstructed from native materials simply by restoring a minimal of physicochemical conditions. Using a membrane extract of human erythroid cells, we have reconstructed a rigid shell structurally supported by a spectrin skeleton fed by ATP and Mg^{2+}, the minimal cofactors necessary for cytoskeleton assembly.[1,19]

Synthetic Reconstruction As Giant Vesicles. We extracted native erythroid membranes obtained from human RBCs from healthy donors (see Specific Methods in Supporting Information, SI). RBCs were first deprived of the whole cytoplasm content, specifically hemoglobin and proteases. Such an erythroid concentrate contained only the membrane component, including the lipid bilayer and the membrane proteins, which are associated with energy metabolism, active transport, and the cytoskeleton. (A biochemical characterization is included as SI.) Much of these proteins develop their specific functions after phosphorylation, thus remaining reversibly inactivated in the ATP-deficient medium resulting after membrane extraction. This membrane extract was then used to create giant proteoliposomes following a specific protocol (Experimental Section) adapted from the procedure previously described by Montes et al.[20] The synthetic vesicles (erythGUVs) were produced at a high yield, morphologically homogeneous and stable under saline conditions, a convenient set of synthetic requirements. When ATP (2 mM final) was added to the suspending buffer medium containing Mg^{2+} (5 mM), a spectrin skeleton instantaneously formed at the outer membrane surface, as revealed by monoclonal antispectrin inmunofluorescence (Figure 1A) congruent with fluorescence lipid labeling (rhodamine-PE; Figure 1B). In the present artificial realization, ATP exhaustion elicited filament disintegration and further network disconnection (Figure 1D), suggesting that actin polymerization under ATP hydrolysis might have a binding role on spectrin filamentation. Prior to ATP addition, we observed randomized material distribution, indicative of full dispersion of

Received: March 26, 2012
Accepted: May 29, 2012
Published: May 29, 2012

dx.doi.org/10.1021/jz300377q | J. Phys. Chem. Lett. 2012, 3, 1583−1588

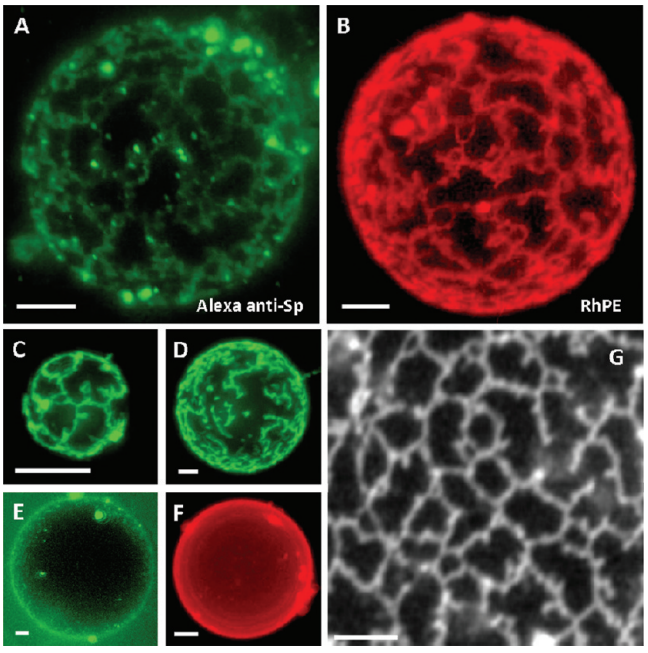

Figure 1. (A,B) 3D-tomographic reconstructions of the skeleton structures artificially formed from lipoprotein membrane extracts of human erythrocytes. The white bar corresponds to 5 μm. (A) Indirect inmunofluorescence image of the spectrin network self-assembled in the presence of ATP (2 mM). Spectrin filaments are visualized in the fluorescence channel corresponding to the secondary Ig antibody Alexa Fluor 488 labeling the human antispectrin monoclonal antibody. A 3D movie can be found in the Supporting Information. (B) Association of lipids to spectrin skeleton visualized by a specific phosphatidyl-ethanolamine lipid probe (Rh-PE). (C) For small vesicles, boundary congruence entails nearly ordered networks to form with a well-defined three-fold branching. (D) Disintegrating network after ATP exhaustion. (E,F) Homogenous erythGUVs in the absence of ATP; under these conditions, spectrin phosphorylation and skeleton assembly are longer inhibited (E: spectrin channel) and lipids (F: Rh-PE lipid channel). (G) Planar bottom transfer of a typical membrane skeleton stuck at the microscope cover slide.

the protein components into the homogeneous lipid mixture (Figure 1E,F). Furthermore, no skeleton was found when spectrin, actin, and ankyrin are specifically removed from the erythroid membrane extract (EME) (see Methods).

Skeleton Structure. We analyzed the structure of the artificial network and compared it with the native cytoskeleton. Figure 1G shows a typical planar image taken at vesicle bottoms supported on the microscope slide. We observed a skeleton made of spectrin filaments (revealed by spectrin inmunofluorescence). The macroscopic filaments found here are thick, abnormally large as compared with native spectrin,[1,19,21] and quite polydisperse in length, a = 2.1 μm ($\pm$0.5 μm; standard deviation, N = 28). These dimensions are consistent with a bundle-like organization probably mediated by the association with fibrilar actin. Indeed, extensive spectrin oligomerization and cross-linking were observed by Cohen et al.[22] in the presence of polymerizing actin.[1,14,15] Graphical analysis performed by ImageJ over a population of different skeletons (SI) revealed a main three-fold connectivity (70%), with a minor concurrence of four-fold coordination nodes (20%). Dimensional analysis revealed two distinct power-law distributions of the node density with the system size ($M \approx L^{-D}$; Figure S4 of the SI). For distances smaller than the characteristic mesh size ($L < a$), the skeleton graphs follow scaling behavior characterized by a fractal dimension, D_S = 1.3 ($\pm$0.1), compatible with the filamentous topology. A higher dimensionality is systematically detected for the wide-range spatial organization (D_B = 1.85 ($\pm$0.10) at $L > a$), suggesting high space completion ($D \approx d = 2$) and high connectivity,[23] confirmed by the negative values of the Euler characteristic of the topological graph ($\chi \ll 0$; Figure S3 of the SI). The analysis of lacunarity indeed demonstrated homogeneous space occupation by the spectrin skeleton ($\Lambda \approx 1$; Figure S5 of the SI). The orientational distributions are characterized by two broad maxima separated by ca. 120° (Figure S6 of the SI), in compatibility with a predominant three-fold connectivity. However, the network is highly disordered, with a very low value of the order parameter of the filament orientations, $S = 2 \langle \cos^2 \theta \rangle - 1 = 0.5$ ($\pm$0.2). The spectrin cytoskeleton

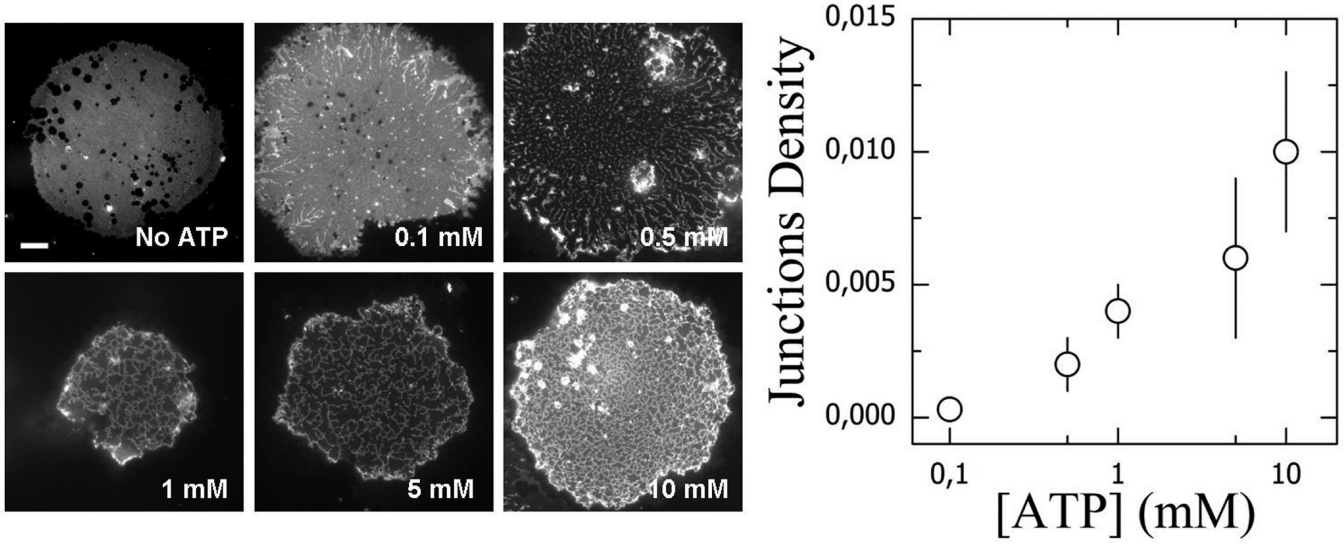

Figure 2. ATP dependence of the area density of junctions in the skeleton assembly. Errors indicate standard deviations over a population of different skeletons obtained at a given ATP concentration (N = 15–20, typically). Each frame in the sequence represents the typical network obtained at every state. The white bar corresponds to 10 microns.

dx.doi.org/10.1021/jz300377q | J. Phys. Chem. Lett. 2012, 3, 1583–1588

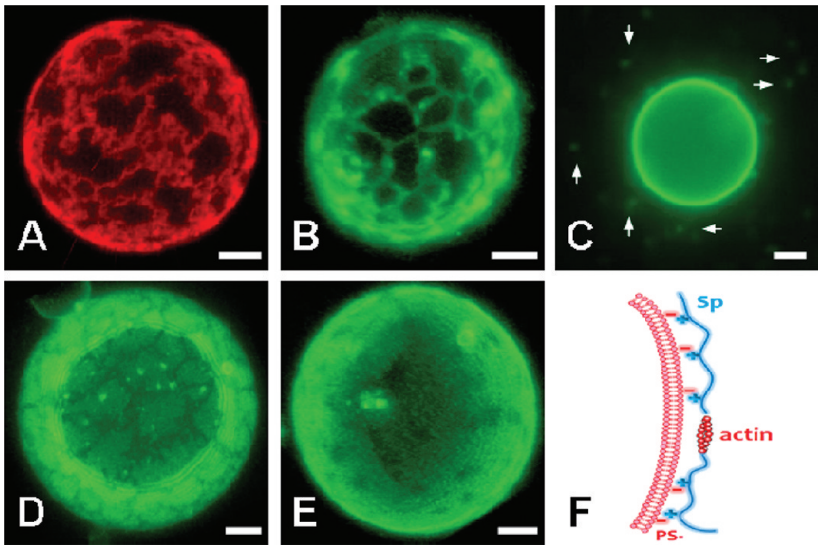

Figure 3. Specific interactions between different fluorescence lipid analogues and the spectrin skeleton assembled in the presence of ATP. The white bar corresponds to 5 μm: (A) Rh-PE and (B) NBD-PS are observed localized with the spectrin skeleton. (C) Electrostatic screening in a high ionic strength dialysis buffer (KCl 500 mM) causes skeleton inhibition and protein detachment by electrostatic disconnection of positive spectrin and the negative membrane containing PS. (The arrows mark some membrane buds ejected from the mother vesicle upon salt addition.) (D) NBD-SM: dark filamentous structures from which the NBD-SM probe is excluded out. (E) NBD-PC: homogeneous distribution of the fluid lipid matrix based on unsaturated phosphatydil-cholines (PC). (Cartoon) Schematic depiction of the electrostatic interaction between the lipid bilayer and the spectrin skeleton.

assembles in vivo as triangular fishnet arrangements forming an adaptable scaffold at the cytoplasm side of the cell membrane. Elemental spectrin filaments are composed of spectrin tetramers (SpT),[21] forming two head-to-head subunits able to bind short actin filaments at the nodes of hexagonal complexes.[14] The present artificial network preserves the microscopic three-fold symmetry based on actin nodes and SpT branches.[14,15] The high polydispersity of filament lengths in conjunction with the higher coordination elements produce together a topological distortion resulting in the disordered structure observed experimentally. Figure 2 reveals the dependence of network connectivities on the nucleotide concentration, a fact indicating that the skeleton assembly is dependent on ATP.

Lipid−Skeleton Interaction. The plasma membrane of human erythrocytes is composed of ∼43% (w/w) of lipids. The four main types of membrane phospholipids are asymmetrically distributed along the outer side (enriched in phosphatidyl-choline (PC) and sphingomyelin (SM)) and the inner side of the bilayer (enriched in phosphatidyl-ethanolamine (PE) and phosphatidyl-serine (PS)).[24,25] This nonrandom distribution is maintained in vivo by active transport supported by amino-phospholipid translocase, a Mg^{2+}-dependent membrane ATPase mediating vectorized transport of PS and PE from the outer to the inner side.[26] Previous studies have revealed strong interaction between spectrin and PE/PS[27] through specific binding sites.[28,29] In the present work, specific spectrin−lipid interactions were detected using fluorescent lipid probes, analogues to the native membrane lipids.

Figure 3 shows the membrane textures observed in the different lipid channels. When PE/PS analogues were visualized, a skeleton-like distribution was observed in the respective fluorescent channels (rhodamine-PE in Figure 3A; NBD-PS in Figure 3B), suggesting cohesive interactions between PE/PS and the spectrin filaments. Electrostatic forces might regulate attractive interactions between the anionic lipid PS and positively charged spectrin. Indeed, electrostatic screening at high ionic strengths (KCl 500 mM) caused the membrane skeleton to detach from the lipid membrane. (See Figure 3C.) The NBD-SM image in Figure 3D displays a negative skeleton replica, indicating SM-segregation from the spectrin localizations. Finally, Figure 3E shows the NBC-PC channel, which displays the ubiquitous distribution of PC, the most abundant component forming the fluid matrix of the lipid bilayer. A homogeneous distribution of PC was observed in this case, suggesting no association of spectrin with this ubiquitous bilayer former, essential for the structural stability of the membrane.

Mechanical Function. The major function of the spectrin skeleton is to provide a rigid shell reinforcing the RBC membrane against stress lysis, thus preserving cell integrity in circulation. Such a mechanical attribute might be preserved in the present artificial skeleton. An accurate measurement of the mechanical parameters was provided from the analysis of the thermal fluctuations, which are controlled by the balance between thermal energy and membrane stiffness.[30] From equipartition, the Helfrich spectrum establishes a dependence $\langle\zeta_q^2\rangle \approx k_BT/(\sigma q^2 + \kappa q^4)$ for the amplitude of the thermal modes. (σ is the lateral tension and κ is the bending rigidity.) Using ultrafast acquisition videomicroscopy in the bright-field mode,[31,32] membrane fluctuations were seen as local changes of the quasi-spherical radius at the equatorial plane, $\zeta_q = \int(\delta R/R_0)e^{iqx}\,dx$. The time-average of the Fourier amplitudes determines the equatorial spectrum, $P_{eq}(q) = \langle\zeta_q^2\rangle$, which might take the form of the azimuth projection of the Helfrich spectrum (SI).

Figure 4A shows a typical experimental spectrum obtained for a homogeneous giant proteoliposome in the absence of ATP. The fluctuation modes closely follow the expected dependence for a bending motion; that is, $P_{eq}(q) \approx q^{-3}$ (SI). Measuring spectra over a population of 20 different vesicles, an average value $\kappa_0 = 90\ (\pm 5)\ k_BT$ was determined for the bending

dx.doi.org/10.1021/jz300377q | J. Phys. Chem. Lett. 2012, 3, 1583−1588

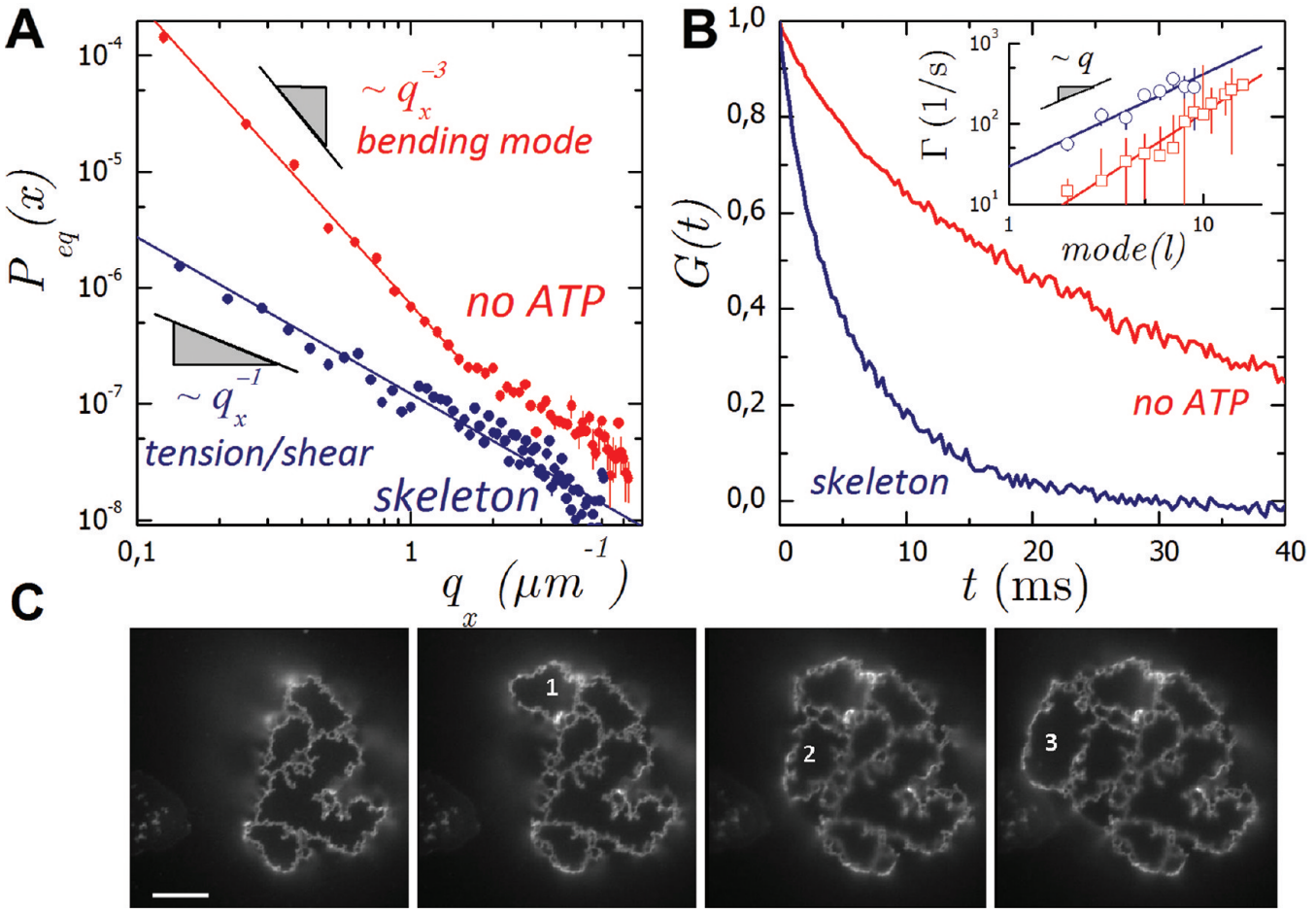

Figure 4. (A) Comparative fluctuation spectra of giant erythroid vesicles before and after skeleton formation. Decreasing fluctuations indicate structural stiffening. (B) Autocorrelation functions of the membrane fluctuations (mode $l = 4$). Inset: q dependence of the relaxation rates: no ATP (red ○); membrane skeleton (blue ○). Lines represent theoretical predictions. (See the text for details.) The error bars correspond to the standard deviation over 20 different vesicles. (C) Consecutive time-sequence of a vesicle-bottom adhesion event of a vesicle with a spectrin skeleton. The white bar corresponds to 10 μm. Numbers mark the neighbor membrane patch incorporated in every next sequence.

modulus. The lateral tension had a low value, $\sigma_0 = 0.17$ (± 0.02) μN/m, typical for lipid vesicles. In the presence of ATP, a connected spectrin skeleton was formed, presumably causing structural stiffness. Consequently, the amplitude of the fluctuations was drastically reduced (by more than a factor of 10 in the low-q regime; Figure 4A). Furthermore, the observed fluctuations turned into a weaker $\sim q^{-1}$ dependence at low q, characteristic of a tension/shear contribution arising from the solid character of the structural skeleton shell[33] (SI). In the presence of the skeleton, a higher bending stiffness $\kappa_{sk} = 120$ (± 11) k_BT ($>\kappa_0$) and lateral tension $\sigma_{sk} = 1.1$ (± 0.2) μN/m (one order of magnitude higher than $\sigma_0 \approx 0.17$ μN/m) were measured, values consistent with the construction of a rigid shell. The presence of the membrane skeleton caused lateral structural stiffening associated with the emergence of finite shear rigidity of the topological network. Indeed, the shear modulus of the ideal triangular network,[30] $\mu = (\sqrt{3}k_{sp}/4)\cdot(1+\sqrt{3}\sigma/k_{sp})$ depends not only on the spring constant (k_{sp}) but also on the strength of the lateral tension (σ). Skeleton stiffening should also affect dynamics. Figure 4B shows the experimental autocorrelation functions of the membrane fluctuations, $G(t) = \langle\zeta_q(0)\zeta_q(t)\rangle$ [see SI]. A much faster relaxation was observed in the presence of the skeleton, corresponding to a stiffer case.[34] The experimental decays nearly followed stretched exponential behavior $G(t) \approx \exp[-(\Gamma t)^{\beta}]$ with $\beta \approx 0.7$, typical of rigid membranes.[32,35] The relaxation rates became faster with increasing stiffness as $\Gamma = (\sigma q + \kappa q^3)/4\eta$. ($\eta$ is the bulk viscosity of the suspending fluid.)[34] In the absence of ATP, the relaxation rates of the lower eigenmodes ($q_l = l/R$, $l = 2, 3...$ up to 12) were characteristic of an intermediate regime $\Gamma \approx q^2$, described well by the formula above. (See the inset in Figure 4B.) In our case, the finite shear rigidity of the shell skeleton caused the lateral tension to increase ($\sigma_{sk} \approx 10\sigma_0$), thus resulting in dynamics dominated by lateral tension $\Gamma_{ATP} \approx \sigma_{sk}q/4\eta$, as observed experimentally (Figure 4B; inset). From a molecular standpoint, high lateral tension and shear resistance are supported by a high conformational persistence of the constituent filaments. The rigid character of the individual filaments is clearly discernible when a single vesicle bottom adheres on the microscope slide (Figure 4C). In the presence of connected skeletons, the process proceeds stepwise; that is, every adhesive event involves a single membrane patch enclosed by a skeleton unit cell, which adheres strongly to the solid surface similar to a hard paving stone.

In summary, although further work is required to elucidate the molecular details, the present results constitute a robust method for the synthetic reconstruction of a cytomimetic skeleton shell with an enhanced rigidity resembling the mechanical function of the native RBC cytoskeleton. Here a

dx.doi.org/10.1021/jz300377q | J. Phys. Chem. Lett. 2012, 3, 1583−1588

strong physiological breakdown was caused in deconstructing the native RBC membranes. However, when minimal components were restored in the system (ATP, Mg^{2+}), an artificial homeostasis was reversibly reverted at assembly conditions. The viability of the present construction demonstrated that each building block had robust surface energetics, specific enough to be selective for their partners but sufficiently versatile to adapt to a broad range of environmental conditions. Noticeably, similar structural rules that govern in vivo the stability of the spectrin cytoskeleton emerged here as a complex interplay of molecular interactions able to regulate self-assembly in a stable artificial microsystem. Therefore, the membrane is able to support mechanical function working as a rigid shell reinforced by the topological skeleton network. From a practical standpoint, such an artificial biomolecular microsystem would define a membrane compartment stable under physiological conditions, rigid enough to support mechanical resilience under external stress and structurally sufficient for artificial membrane realizations, thus opening promising synthetic opportunities.

EXPERIMENTAL SECTION

The EME was extracted from human blood obtained in fresh from healthy donors. Aliquots were stored frozen at −20 °C. Giant vesicles made of EME, or EME devoid the membrane proteins spectrin and ankyrin (EME Sp^- Ank^-), were prepared by electroformation.[36] (See the Supporting Information - Materials and Specific Methods for details of chemicals and extraction/characterization methods.) The fabrication chamber is composed of two conductor indium tin oxide (ITO)-coated glass slides (7.5 × 2.5 cm^2; 15−25 Ω/sq surface resistivity, Sigma) separated 0.5 mm by a Teflon/Bytac spacer. The EME suspension was slowly thawed at room temperature. Then, 10 μL was spread over a rectangular area (1.5 × 2.5 cm^2) on both conductor surfaces. After aqueous solvent evaporation, the fabrication chamber was sealed using Vitrex paste. Then, the films were rehydrated in sucrose solution (200 mM) and the electrodes were connected to an AC power supply (8 Hz, 1.1 V) for 2 h. Giant vesicles (erythGUVs) were obtained almost spherical, with a variable size ranging from a few up to several tens micrometers. The observation chamber was composed of two circular microscope cover slides (ϕ25 mm) separated by a PDMS ring spacer (2.5 mm thickness). To avoid vesicle adhesion and breakage, the chamber bottom was incubated for 20 min with casein solution (0.5% w/w). After chamber washing out, a drop (40 μL) of isosmolar buffer solution (75 mM NaCl, 40 mM glucose, 10 mM Hepes, 5 mM $MgCl_2$, 1 mM KCl, pH 7,4) is placed at the center of the observation chamber. The density difference between the sugar medium outside (glucose) and inside (sucrose) allowed the vesicles to sediment in the observation chamber, also providing a better optical contrast for bright-field microscopy. Then, 10 μL of erythGUV suspension (containing ATP (2 mM final) when necessary) was transferred to the observation chamber, which was immediately sealed with a cover glass to avoid for evaporation and consequent osmotic stress. Vesicles were observed in an inverted optical microscope (Nikon Eclipse TE2000, objective oil immersion 63×) equipped with a cooled CCD camera (Nikon DS-1QM, 14 fps, 1 Mpixel). Fluorescent labeling (see SI) allowed molecular visualization under fluorescence microscopy (using a 100 W Hg lamp and FITC and Texas Red filter sets). Three-dimensional tomographic images were reconstructed from a stack of slide images captured at different focal planes (with a typical *z*-step of 0.7 μm) using a Nikon nanoposition accessory with a high *z*-resolution (50 nm). Images stacks were deconvoluted in the Nikon's imaging software NIS-elements to finally obtain 3D tomographic reconstructions.

ASSOCIATED CONTENT

Supporting Information

Materials and specific methods, graph analysis, fluctuation analysis, and movie with the structure of a spectrin skeleton supported on a giant vesicle. This material is available free of charge via the Internet http://pubs.acs.org.

AUTHOR INFORMATION

Corresponding Author

*E-mail: monroy@quim.ucm.es; ivanlopez@quim.ucm.es.

Notes

The authors declare no competing financial interest.

ACKNOWLEDGMENTS

We thank J. L. Carrascosa and V. Muñoz for comments on the manuscript. We are grateful to UCM Medical Service (*Medicina del Trabajo*) for blood extractions. This work was funded by MICINN under grants FIS2009-14650-C02-01 and Consolider-Ingenio 2010 "Nanociencia Molecular" (CSD2007-0010), and S2009MAT-1507 (NOBIMAT) from CAM. I.L.-M. was supported by *Juan de la Cierva* program (MICINN).

REFERENCES

(1) Alberts, B.; Johnson, A.; Lewis, J.; Raff, M.; Roberts, K.; Walter, P.; Bray, D.; Watson, J. *Molecular Biology of the Cell*, 5th ed.; Garland Science: New York, 2008.

(2) Ball, P. Synthetic Biology: Starting from Scratch. *Nature* **2004**, *431*, 624−626.

(3) Gibson, D. G.; Glass, J. I.; Lartigue, C.; Noskov, V. N.; Chuang, R. Y.; Algire, M. A.; Benders, G. A.; Montague, M. G.; Ma, L.; Moodie, M. M. Creation of a Bacterial Cell Controlled by a Chemically Synthesized Genome. *Science* **2010**, *329*, 52.

(4) Noireaux, V.; Maeda, Y. T.; Libchaber, A. Development of an Artificial Cell, From Self-Organization to Computation and Self-Reproduction. *Proc. Natl. Acad. Sci. U.S.A.* **2011**, *108*, 3473−3480.

(5) Liu, A. P.; Fletcher, D. A. Biology under Construction: In Vitro Reconstitution of Cellular Function. *Nat. Rev. Mol. Cell Biol.* **2009**, *10*, 644−650.

(6) Fletcher, D. A.; Mullins, R. D. Cell Mechanics and the Cytoskeleton. *Nature* **2010**, *463*, 485−492.

(7) Häckl, W.; Bärmann, M.; Sackmann, E. Shape Changes of Self-Assembled Actin Bilayer Composite Membranes. *Phys. Rev. Lett.* **1998**, *80*, 1786−1789.

(8) Helfer, E.; Harlepp, S.; Bourdieu, L.; Robert, J.; MacKintosh, F.; Chatenay, D. Microrheology of Biopolymer-Membrane Complexes. *Phys. Rev. Lett.* **2000**, *85*, 457−460.

(9) Bausch, A.; Kroy, K. a Bottom-up Approach to Cell Mechanics. *Nat. Phys.* **2006**, *2*, 231−238.

(10) Liu, A. P.; Richmond, D. L.; Maibaum, L.; Pronk, S.; Geissler, P. L.; Fletcher, D. A. Membrane-Induced Bundling of Actin Filaments. *Nat. Phys.* **2008**, *4*, 789−793.

(11) Pontani, L. L.; Van der Gucht, J.; Salbreux, G.; Heuvingh, J.; Joanny, J. F.; Sykes, C. Reconstitution of an Actin Cortex Inside a Liposome. *Biophys. J.* **2009**, *96*, 192−198.

(12) Tsai, F. C.; Stuhrmann, B.; Koenderink, G. H. Encapsulation of Active Cytoskeletal Protein Networks in Cell-Sized Liposomes. *Langmuir* **2011**, *27*, 10061−10071.

(13) Merkle, D.; Kahya, N.; Schwille, P. Reconstitution and Anchoring of Cytoskeleton Inside Giant Unilamellar Vesicles. *ChemBioChem* **2008**, *9*, 2673−2681.
(14) Byers, T. J.; Branton, D. Visualization of the Protein Associations in the Erythrocyte Membrane Skeleton. *Proc. Natl. Acad. Sci. U.S.A.* **1985**, *82*, 6153−6157.
(15) Shen, B. W.; Josephs, R.; Steck, T. L. Ultrastructure of the Intact Skeleton of the Human Erythrocyte Membrane. *J. Chem. Biol.* **1986**, *102*, 997−1006.
(16) Whitesides, G. M.; Grzybowski, B. Self-Assembly at All Scales. *Science* **2002**, *295*, 2418−2421.
(17) Glotzer, S. C. Materials Science. Some Assembly Required. *Science* **2004**, *306*, 419−420.
(18) Hormoz, S.; Brenner, M. P. Design Principles for Self-Assembly with Short-Range Interactions. *Proc. Natl. Acad. Sci. U.S.A.* **2011**, *108*, 5193−5198.
(19) Yawata, Y. *Cell Membrane: The Red Blood Cell as a Model*; Wiley-VCH: Weinheim, Germany, 2003.
(20) Montes, L. R.; Alonso, A.; Bagatolli, L. A. Giant Unilamellar Vesicles Electroformed from Native Membranes and Organic Lipid Mixtures under Physiological Conditions. *Biophys. J.* **2007**, *93*, 3548−3554.
(21) Morrow, J.; Marchesi, V. Self-Assembly of Spectrin Oligomers in Vitro: A Basis for a Dynamic Cytoskeleton. *J. Chem. Biol.* **1981**, *88*, 463.
(22) Cohen, C. M.; Tyler, J. M.; Branton, D. Spectrin-Actin Associations Studied by Electron Microscopy of Shadowed Preparations. *Cell* **1980**, *21*, 875−883.
(23) Song, C.; Havlin, S.; Makse, H. A. Self-Similarity of Complex Networks. *Nature* **2005**, *433*, 392−395.
(24) Bretscher, M. S. Asymmetrical Lipid Bilayer Structure for Biological Membranes. *Nature* **1972**, *236*, 11−12.
(25) Verkleij, A.; Zwaal, R.; Roelofsen, B.; Comfurius, P.; Kastelijn, D.; Van Deenen, L. The Asymmetric Distribution of Phospholipids in the Human Red Cell Membrane. A Combined Study Using Phospholipases and Freeze-Etch Electron Microscopy. *Biochim. Biophys. Acta, Biomembr.* **1973**, *323*, 178−193.
(26) Seigneuret, M.; Devaux, P. F. ATP-Dependent Asymmetric Distribution of Spin-Labeled Phospholipids in the Erythrocyte Membrane: Relation to Shape Changes. *Proc. Natl. Acad. Sci. U.S.A.* **1984**, *81*, 3751−3755.
(27) Sikorski, A. F.; Michalak, K.; Bobrowska, M. Interaction of Spectrin with Phospholipids. Quenching of Spectrin Intrinsic Fluorescence by Phospholipid Suspensions. *Biochim. Biophys. Acta, Biomembr.* **1987**, *904*, 55−60.
(28) Hryniewicz-Jankowska, A.; Bok, E.; Dubielecka, P.; Chorzalska, A.; Diakowski, W.; Jezierski, A.; Lisowski, M.; Sikorski, A. F. Mapping of an Ankyrin-Sensitive, Phosphatidylethanolamine/Phosphatidylcholine Mono-and Bi-Layer Binding Site in Erythroid -Spectrin. *Biochem. J.* **2004**, *382*, 677−685.
(29) An, X.; Guo, X.; Sum, H.; Morrow, J.; Gratzer, W.; Mohandas, N. Phosphatidylserine Binding Sites in Erythroid Spectrin: Location and Implications for Membrane Stability. *Biochemistry* **2004**, *43*, 310−315.
(30) Boal, D. H. *Mechanics of the Cell*; Cambridge University Press: Cambridge, U.K., 2002.
(31) Pecreaux, J.; Dobereiner, H. G.; Prost, J.; Joanny, J. F.; Bassereau, P. Refined Contour Analysis of Giant Unilamellar Vesicles. *Eur. Phys. J. E* **2004**, *13*, 277−290.
(32) Rodríguez-García, R.; Mell, M.; López-Montero, I.; Monroy, F. Subdiffusive Fluctuation Dynamics of Rigid Membranes As Resolved by Ultrafast Videomicroscopy. *Europhys. Lett.* **2011**, *94*, 28009.
(33) Auth, T.; Safran, S. A.; Gov, N. S. Fluctuations of Coupled Fluid and Solid Membranes with Application to Red Blood Cells. *Phys. Rev. E* **2007**, *76*, 051910.
(34) Milner, S. T.; Safran, S. A. Dynamical Fluctuations of Droplet Microemulsions and Vesicles. *Phys. Rev. A* **1987**, *36*, 4371−4379.
(35) Zilman, A. G.; Granek, R. Undulations and Dynamic Structure Factor of Membranes. *Phys. Rev. Lett.* **1996**, *77*, 4788−4791.
(36) Mathivet, L.; Cribier, S.; Devaux, P. F. Shape Change and Physical Properties of Giant Phospholipid Vesicles Prepared in the Presence of an AC Electric Field. *Biophys. J.* **1996**, *70*, 1112−1121.